Thermodynamic stabilization of nanocrystalline binary alloys

Mostafa Saber, Hasan Kotan, Carl C. Koch, and Ronald O. Scattergood

View Online   Export Citation   CrossMark

ARTICLES YOU MAY BE INTERESTED IN

A predictive model for thermodynamic stability of grain size in nanocrystalline ternary alloys
Journal of Applied Physics **114**, 103510 (2013); https://doi.org/10.1063/1.4821040

Ultrahigh strength and high ductility of bulk nanocrystalline copper
Applied Physics Letters **87**, 091904 (2005); https://doi.org/10.1063/1.2034122

Rapid stress-driven grain coarsening in nanocrystalline Cu at ambient and cryogenic temperatures
Applied Physics Letters **87**, 061921 (2005); https://doi.org/10.1063/1.2008377

Thermodynamic stabilization of nanocrystalline binary alloys

Mostafa Saber,[a)] Hasan Kotan, Carl C. Koch, and Ronald O. Scattergood
Department of Materials Science and Engineering, North Carolina State University, 911 Partners Way, Room 3002, Raleigh, North Carolina 27695-7907, USA

The work presented here was motivated by the need to develop a predictive model for thermodynamic stabilization of binary alloys that is applicable to strongly segregating size-misfit solutes, and that can use available input data for a wide range of solvent-solute combinations. This will serve as a benchmark for selecting solutes and assessing the possible contribution of thermodynamic stabilization for development of high-temperature nanocrystalline alloys. Following a regular solution model that distinguishes the grain boundary and grain interior volume fractions by a transitional interface in a closed system, we include both the chemical and elastic strain energy contributions to the mixing enthalpy ΔH_{mix} using an appropriately scaled linear superposition. The total Gibbs mixing free energy ΔG_{mix} is minimized with respect to simultaneous variations in the grain-boundary volume fraction and the solute contents in the grain boundary and grain interior. The Lagrange multiplier method was used to obtain numerical solutions with the constraint of fixed total solute content. The model predictions are presented using a parametric variation of the required input parameters. Applications are then given for the dependence of the nanocrystalline grain size on temperature and total solute content for selected binary systems where experimental results suggest that thermodynamic stabilization could be effective. © 2013 American Institute of Physics. [http://dx.doi.org/10.1063/1.4791704]

I. INTRODUCTION

Grain boundaries in nanocrystalline microstructures produce a significant increase in the total free energy of the system. The presence of a large driving force for grain growth due to a decrease in grain boundary content can therefore be expected.[1] Kinetic stabilization and thermodynamic stabilization are the two basic mechanisms by which stability of a nanoscale grain size can be retained at high temperatures in alloys. Kinetic stabilization is achieved by reducing the mobility of grain boundaries by solute drag, second-phase particle pinning (Zener pining), or other mechanisms such as porosity drag. The kinetic mechanisms involve thermally activated processes and therefore grain growth will occur as a function of both time and temperature. Thermodynamic stabilization involves a metastable equilibrium state, and alloy mixing entropy ΔS_{mix} will produce a temperature dependent grain size. Weissmuller[2,3] developed the concept of thermodynamic stabilization using the Gibbs absorption equation. This leads to relations of the form

$$\gamma = \frac{dG}{dA} = \gamma_0 + \Gamma_s[\Delta H_{seg} - T\Delta S_{seg}]. \qquad (1)$$

γ_0 is the initial non-segregated grain boundary energy, Γ_s is the solute excess at the interface, ΔH_{seg} is the segregation enthalpy, and ΔS_{seg} is the segregation entropy. γ is defined to be the change in free energy dG with respect to variation in grain boundary area dA in a closed system. This equation is often used to define thermodynamic stabilization as the condition where γ is lowered to be zero. If γ is assumed to be the

cohesive grain boundary energy, grain boundary cohesion is lost and grains would separate at the stabilization point ($\gamma = 0$). Based on zero creep measurements, cohesive grain boundary energy varies with the increasing global solute content and grain boundary energy reaches a non-zero limit.[4] The definition of grain boundary energy from Eq. (1) is restricted to a dilute solution containing a negligible volume fraction of interface. In a nanocrystalline microstructure, the volume fraction of grain boundary will be significant and there is no restriction on the bulk solute concentration. The model considered in this paper does not follow the criterion for thermodynamic stabilization based on Eq. (1).

Numerous experimental studies have shown that solute addition stabilizes a nanoscale grain size at higher temperatures; however in most investigations, there is no direct evidence to reveal which mechanisms are effective.[5–13] Analytical models have been proposed to deal with the phenomenon of interface segregation. McLean[14] assumed that the enthalpy of segregation (ΔH_{seg}) was the complete release of the elastic strain energy associated with the solute atomic size misfit, i.e., $\Delta H_{seg} = -\Delta E_{els}$. The elastic mistfit strain energy (ΔE_{els}) per solute atom A for an AB alloy containing N_o atoms is obtained using a model due to Friedel[15]

$$\Delta E_{els} = \frac{2K_A G_B (V_A - V_B)^2}{3K_A V_B + 4G_B V_A}. \qquad (2)$$

K_A is the bulk solute modulus, G_B is the solvent shear modulus, and V_A and V_B are the atomic volumes of pure solute and solvent, respectively. Defay *et al.*[16] expressed the segregation enthalpy in terms of chemical contributions using a regular solution model, i.e., $\Delta H_{seg} = \Delta H_{chem}$. It was pointed out that neither the McLean[14] nor the Defay *et al.*[16] models

---

[a)]Author to whom correspondence should be addressed. Electronic mail: msaber@ncsu.edu. Tel.: +1-919-515-2377. Fax: +1-919-515-7724.

provide correct predictions of the grain boundary segregation in a binary alloy.[17] The reason is that the model due to Defay *et al.*[16] considers only the chemical contributions to the segregation enthalpy, whereas McLean[14] excludes all but the elastic contributions. Wynblatt and Ku (WK)[18,19] recognized these limitations and proposed a model in which the chemical and elastic contributions to the segregation enthalpy are combined linearly

$$\Delta H_{seg} = \Delta H_{chem} + \Delta H_{els}. \quad (3)$$

Trelewicz and Schuh (TS)[20] developed a regular solution model for thermodynamic stabilization of nanocrystalline alloys. They distinguished the grain boundary region from the grain interior region by a transitional interface and applied the regular solution approximation for each region. The equilibrium condition is obtained by minimization of the total Gibbs mixing free energy with respect to simultaneous variations in the grain boundary composition and the grain boundary volume fraction. This approach provides a more rigorous analytical modeling framework for evaluating nanoscale grain size stability. Analogous to the Defay *et al.*[16] model, the TS model does not also take the elastic part of the enthalpy into account. The elastic term always contributes to grain-boundary segregation whereas the chemical term may contribute or detract. Therefore, addition of elastic strain energy to the enthalpy change is essential for strongly segregating alloys systems involving large size misfit (non-equilibrium) solute additions. Recently, Chookajorn *et al.*[21] have suggested a modification incorporating the elastic strain energy into the total enthalpy of segregation (ΔH_{seg}). However, the enthalpy of segregation (as a derivative of the enthalpy of mixing (ΔH_{mix}) with respect to the atomic fraction of solute at grain boundary) was not properly scaled by the volume fraction of the grain boundary region. Objectives of this work are to include the elastic term into a regular solution model and to minimize the Gibbs free energy with respect to all the variables simultaneously contributing to the segregation and grain growth. This approach offers a rational solution for the equilibrium condition for a nanocrystalline system. The cohesive grain boundary energy never becomes zero. A numerical solution method is presented based on the Lagrange multiplier technique. This is readily implemented using standard software packages.

II. ANALYTICAL TREATMENT

A regular solution model for the chemical contribution is developed as a sum of the atomic bond energies for different regions. The components of the model are described next in terms of mixing energy changes.

A. Internal energy of mixing

Following the TS approach using similar notation, the volume of the system is divided into bulk (grain interior) and intergranular (grain boundary) regions connected by transitional bonds as illustrated in Figure 1. An atomic bond interaction energy for each region can be defined using the regular solution model. The total internal energy of the system is obtained by
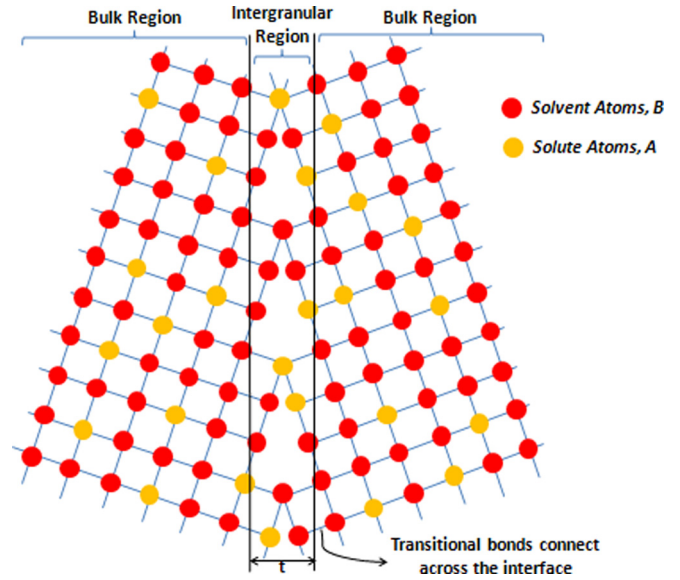

FIG. 1. The schematic of separated bonding regions of a system of two grains and a boundary with thickness *t*.

adding the bond energies for the different regions. Assuming a binary mixture of solute *A* and solvent *B* atoms gives

$$
\begin{aligned}
U_{soln.} = &\; N_b^{AA}E^{AA} + N_b^{BB}E^{BB} + N_b^{AB}E^{AB} \\
&+ \alpha(N_t^{AA}E^{AA} + N_t^{BB}E^{BB} + N_t^{AB}E^{AB}) \\
&+ \alpha(N_{ig}^{AA}E^{AA} + N_{ig}^{BB}E^{BB} + N_{ig}^{AB}E^{AB}).
\end{aligned} \quad (4)
$$

N_k^{ij} is the number of bonds in each region and E^{ij} is the bond energy where the superscripts (ij) distinguish the bond type in terms of like or unlike pairs of *A* and *B*, and the subscript (k) denotes the bulk (b), transitional (t), and intergranular (ig) regions. The α multiplier is introduced to distinguish the bond energy in the intergranular and transitional regions from the bulk region. The αE^{ij} terms are the equivalent of E_{ig} in the TS model.

The internal energy of mixing arises from the difference between internal energy of the solution and a reference state

$$\Delta U_{mix} = U_{soln} - U_{ref}. \quad (5)$$

The reference state is defined as an unmixed and interface-free state of the system with the same *AB* composition. The regular solution model for the reference state gives

$$U_{ref} = \frac{z}{2}N_{total}^A E^{AA} + \frac{z}{2}N_{total}^B E^{BB}. \quad (6)$$

N_{total}^A and N_{total}^B are the total numbers of pure solute and solvent atoms in the system, respectively, and *z* is the coordination number of the solvent atom. In a system with a given *AB* composition, the total number of *A* and *B* atoms is related to the number of bonds by

$$
\begin{aligned}
zN_{total}^A &= 2N_b^{AA} + 2N_t^{AA} + 2N_{ig}^{AA} + N_b^{AB} + N_t^{AB} + N_{ig}^{AB} \\
zN_{total}^B &= 2N_b^{BB} + 2N_t^{BB} + 2N_{ig}^{BB} + N_b^{AB} + N_t^{AB} + N_{ig}^{AB}.
\end{aligned} \quad (7)
$$

The substitution of $N_{total}{}^A$ and $N_{total}{}^B$ from Eq. (7) into Eq. (6) followed by the substitution of Eq. (6) into Eq. (5) leads to

$$\Delta U_{mix} = N_b^{AB}\left(E^{AB} - \frac{E^{AA}+E^{BB}}{2}\right)$$
$$+ (N_t^{AB} + N_{ig}^{AB})\left(\alpha E^{AB} - \frac{E^{AA}+E^{BB}}{2}\right)$$
$$+ (\alpha - 1)\left((N_t^{AA} + N_{ig}^{AA})E^{AA} + (N_t^{BB} + N_{ig}^{BB})E^{BB}\right) \quad (8)$$

ΔU_{mix} can be rearranged to give

$$\Delta U_{mix} = N_b^{AB}\left(E^{AB} - \frac{E^{AA}+E^{BB}}{2}\right)$$
$$+ \alpha(N_t^{AB} + N_{ig}^{AB})\left(E^{AB} - \frac{E^{AA}+E^{BB}}{2}\right)$$
$$+ (\alpha - 1)\left(N_t^{AA}E^{AA} + N_t^{BB}E^{BB} + N_t^{AB}\left(\frac{E^{AA}+E^{BB}}{2}\right)\right)$$
$$+ (\alpha - 1)\left(N_{ig}^{AA}E^{AA} + N_{ig}^{BB}E^{BB} + N_{ig}^{AB}\left(\frac{E^{AA}+E^{BB}}{2}\right)\right). \quad (9)$$

The regular solution interaction energy parameter ω is defined as

$$\omega = \left(E^{AB} - \frac{E^{AA} - E^{BB}}{2}\right). \quad (10)$$

Therefore,

$$\Delta U_{mix} = \omega N_b^{AB}$$
$$+ \alpha\omega(N_t^{AB} + N_{ig}^{AB})$$
$$+ (\alpha - 1)\left(N_t^{AA}E^{AA} + N_t^{BB}E^{BB} + N_t^{AB}\left(\frac{E^{AA}+E^{BB}}{2}\right)\right)$$
$$+ (\alpha - 1)\left(N_{ig}^{AA}E^{AA} + N_{ig}^{BB}E^{BB} + N_{ig}^{AB}\left(\frac{E^{AA}+E^{BB}}{2}\right)\right). \quad (11)$$

In a three-dimensional polycrystal with grain size d, grain-boundary thickness t and a grain-shape factor proportional to d, the intergranular volume fraction f_{ig} of the grain boundary region can be given as[22]

$$f_{ig} = 1 - \left(\frac{d-t}{d}\right)^3. \quad (12)$$

Mass conservation for the solute contents (atom fractions) X_{ig}, X_b, and X_0 in the intergranular region, bulk region, and total system, respectively, requires the constraint condition

$$X_b(1 - f_{ig}) + X_{ig}f_{ig} = X_0. \quad (13)$$

The total number of bonds N_b^{ij} in the bulk region can be expressed as a function of f_{ig}, the total number of atoms N_0 in the system, and the coordination number z

$$N_b^{ij} = \frac{z}{2}N_0(1 - f_{ig}). \quad (14a)$$

The factor v is defined as the effective bond coordination contributing to the transitional bonding region in Figure 1. Therefore, the total number of transitional bonds N_t^{ij} is

$$N_t^{ij} = vzN_0f_{ig}. \quad (14b)$$

Since $N_0 = 2N_b^{ij} + 2N_t^{ij} + 2N_{ig}^{ij}$, the total number of intergranular bonds N_{ig}^{ij} is obtained as

$$N_{ig}^{ij} = \frac{(1-2v)z}{2}N_0f_{ig}. \quad (14c)$$

The existence probabilities P_k^{ij} for bonds can be given in terms of solute contents in the respective regions as follows:

$$P_b^{AB} = 2X_b(1 - X_b), \quad (15a)$$
$$P_t^{AA} = X_bX_{ig}, \quad (15b)$$
$$P_t^{BB} = (1 - X_b)(1 - X_{ig}), \quad (15c)$$
$$P_t^{AB} = X_b(1 - X_{ig}) + X_{ig}(1 - X_b), \quad (15d)$$
$$P_{ig}^{AA} = X_{ig}^2, \quad (15e)$$
$$P_{ig}^{BB} = (1 - X_{ig})^2, \quad (15f)$$
$$P_{ig}^{AB} = 2X_{ig}(1 - X_{ig}). \quad (15g)$$

The number of bonds for like and/or unlike pairs can be calculated from the total number of bonds multiplied by the existence probability in each of the respective regions

$$N_b^{AB} = P_b^{AB} \times N_b^{ij} = zN_0X_b(1 - X_b)(1 - f_{ig}), \quad (16a)$$
$$N_t^{AA} = P_t^{AA} \times N_t^{ij} = vzN_0X_bX_{ig}f_{ig}, \quad (16b)$$
$$N_t^{BB} = P_t^{BB} \times N_t^{ij} = vzN_0(1 - X_b)(1 - X_{ig})f_{ig}, \quad (16c)$$
$$N_t^{AB} = P_t^{AB} \times N_t^{ij} = vzN_0\left(X_b(1 - X_{ig}) + X_{ig}(1 - X_b)\right)f_{ig}, \quad (16d)$$
$$N_{ig}^{AA} = P_{ig}^{AA} \times N_{ig}^{ij} = \frac{(1-2v)z}{2}N_0X_{ig}^2f_{ig}, \quad (16e)$$
$$N_{ig}^{BB} = P_{ig}^{BB} \times N_{ig}^{ij} = \frac{(1-2v)z}{2}N_0(1 - X_{ig})^2f_{ig}, \quad (16f)$$
$$N_{ig}^{AB} = P_{ig}^{AB} \times N_{ig}^{ij} = (1-2v)zN_0X_{ig}(1 - X_{ig})f_{ig}. \quad (16g)$$

Substituting these into Eq. (11) gives ΔU_{mix} per atom

$$\frac{\Delta U_{mix}}{N_0} = \omega zX_b(1 - X_b)(1 - f_{ig})$$
$$+ \alpha\omega vz\left(X_b(1 - X_{ig}) + X_{ig}(1 - X_b)\right)f_{ig}$$
$$+ \frac{(\alpha-1)vz}{2}\left((X_b + X_{ig})E^{AA} + (1 - X_b + 1 - X_{ig})E^{BB}\right)f_{ig}$$
$$+ \alpha\omega(1 - 2v)zX_{ig}(1 - X_{ig})f_{ig}$$
$$+ \frac{(\alpha-1)(1-2v)z}{2}(X_{ig}E^{AA} + (1 - X_{ig})E^{BB})f_{ig}. \quad (17)$$

If the $(\alpha - 1)zE^{ij}$ terms are rearranged as follows:

$$\frac{(\alpha - 1)z}{2}E^{AA} = \frac{\alpha z}{2}E^{AA} - \frac{z}{2}E^{AA}, \quad (18a)$$

$$\frac{(\alpha - 1)z}{2}E^{BB} = \frac{\alpha z}{2}E^{BB} - \frac{z}{2}E^{BB}, \quad (18b)$$

they can be interpreted as differences in the energies between intergranular and bulk bonds. These can be related to the cohesive grain boundary energies of pure elements of A and B

$$\frac{(\alpha - 1)z}{2}E^{AA} = \sigma\gamma^A, \quad (19a)$$

$$\frac{(\alpha - 1)z}{2}E^{BB} = \sigma\gamma^B. \quad (19b)$$

σ is defined as the molar grain boundary area, which is taken to be

$$\sigma = N_{Avg}(V^B)^{\frac{2}{3}}. \quad (20)$$

N_{Avg} is Avogadro's number and V^B is the atomic volume of the solvent atom. ΔU_{mix} can then be reduced to

$$\frac{\Delta U_{mix}}{N_0} = \omega z X_b(1 - X_b)(1 - f_{ig})$$
$$+ \alpha \omega v z \Big(X_b(1 - X_{ig}) + X_{ig}(1 - X_b)\Big)f_{ig}$$
$$+ v\sigma\Big((X_b + X_{ig})\gamma^A + (1 - X_b + 1 - X_{ig})\gamma^B\Big)f_{ig}$$
$$+ \alpha\omega(1 - 2v)z X_{ig}(1 - X_{ig})f_{ig}$$
$$+ (1 - 2v)\sigma\Big(X_{ig}\gamma^A + (1 - X_{ig})\gamma^B\Big)f_{ig}. \quad (21)$$

B. Enthalpy of mixing

If the volume change caused by mixing is neglected, the enthalpy change is equivalent to the internal energy change at fixed temperature and pressure

$$\Delta H = \Delta U + P\Delta V = \Delta U. \quad (22)$$

ΔU_{mix} in Eq. (21) corresponds to the chemical energy change. An elastic internal energy change (ΔU_{els}) due to solute atom size misfit must be added to ΔU_{mix} to get the total enthalpy of mixing

$$\frac{\Delta H_{mix}}{N_0} = \frac{\Delta U_{mix}}{N_0} + \frac{\Delta U_{els}}{N_0}. \quad (23)$$

It is assumed that when a solute atom segregates to a grain boundary, the total elastic strain energy is released. Therefore, the elastic internal energy change per atom for introducing an atom fraction X_{ig} of misfit solute atoms into the grain boundary region is obtained by an elastic strain energy term (ΔH_{els}) which must be scaled by X_{ig} and f_{ig}

$$\frac{\Delta U_{els}}{N_0} = X_{ig}\Delta H_{els}f_{ig}. \quad (24)$$

$\Delta H_{els} = -\Delta E_{els}$ will be obtained from Eq. (2).

The total enthalpy of mixing is obtained by combining Eqs. (21) and (24) via Eq. (23)

$$\frac{\Delta H_{mix}}{N_0} = \omega z X_b(1 - X_b)(1 - f_{ig})$$
$$+ \alpha\omega v z (X_b(1 - X_{ig}) + X_{ig}(1 - X_b))f_{ig}$$
$$+ v\sigma\Big((X_b + X_{ig})\gamma^A + (1 - X_b + 1 - X_{ig})\gamma^B\Big)f_{ig}$$
$$+ \alpha\omega(1 - 2v)z X_{ig}(1 - X_{ig})f_{ig}$$
$$+ (1 - 2v)\sigma(X_{ig}\gamma^A + (1 - X_{ig})\gamma^B)f_{ig}$$
$$+ X_{ig}\Delta H_{els}f_{ig}. \quad (25)$$

C. Free energy of mixing

The entropy change due to mixing will be approximated by the ideal AB solid solution entropy, i.e., no excess entropy terms are included

$$\frac{\Delta S_{mix}}{N_0} = -R[X_b\ln(X_b) + (1 - X_b)\ln(1 - X_b)](1 - f_{ig})$$
$$- R[X_{ig}\ln(X_{ig}) + (1 - X_{ig})\ln(1 - X_{ig})]f_{ig}. \quad (26)$$

The Gibbs free energy of mixing is

$$\frac{\Delta G_{mix}}{N_0} = \frac{\Delta H_{mix}}{N_0} - \frac{T\Delta S_{mix}}{N_0}. \quad (27)$$

Substituting Eqs. (25) and (26) into Eq. (27) gives the final result

$$\frac{\Delta G_{mix}}{N_0} = \omega z X_b(1 - X_b)(1 - f_{ig})$$
$$+ \alpha\omega v z \Big(X_b(1 - X_{ig}) + X_{ig}(1 - X_b)\Big)f_{ig}$$
$$+ v\sigma\Big((X_b + X_{ig})\gamma^A + (1 - X_b + 1 - X_{ig})\gamma^B\Big)f_{ig}$$
$$+ \alpha\omega(1 - 2v)z X_{ig}(1 - X_{ig})f_{ig}$$
$$+ (1 - 2v)\sigma(X_{ig}\gamma^A + (1 - X_{ig})\gamma^B)f_{ig}$$
$$+ X_{ig}\Delta H_{els}f_{ig}$$
$$+ RT[X_b\ln(X_b) + (1 - X_b)\ln(1 - X_b)](1 - f_{ig})$$
$$+ RT[X_{ig}\ln(X_{ig}) + (1 - X_{ig})\ln(1 - X_{ig})]f_{ig}. \quad (28)$$

The parameters ω, α, v, z, σ, ΔH_{els}, γ^A, γ^B, R, and T will be specified for a given AB alloy. ΔG_{mix} in Eq. (28) is then a function of the three variables X_b, X_{ig}, and f_{ig}.

D. Equilibrium condition

The equilibrium state is obtained by simultaneous minimization of ΔG_{mix} with respect to X_b, X_{ig}, and f_{ig}

$$\frac{1}{N_0}\frac{\partial \Delta G_{mix}}{\partial X_b} = 0, \quad (29a)$$

$$\frac{1}{N_0}\frac{\partial \Delta G_{mix}}{\partial X_{ig}} = 0, \quad (29b)$$

$$\frac{1}{N_0}\frac{\partial \Delta G_{mix}}{\partial f_{ig}} = 0, \quad (29c)$$

subject to the constraint condition,

$$X_b(1 - f_{ig}) + X_{ig}f_{ig} - X_0 = 0. \qquad (30)$$

It should be emphasized that a thermodynamic stabilization requires the full solution to Eqs. (29a)–(29c) and (30).

Numerical solutions are obtained here using the Lagrange multiplier technique. The Lagrangian L is defined as

$$L = \frac{\Delta G_{mix}}{N_0} - \lambda(X_b(1 - f_{ig}) + X_{ig}f_{ig} - X_0). \qquad (31)$$

λ is the Lagrangian multiplier. Recognizing that X_b, X_{ig}, f_{ig}, and λ are treated as independent variables for L, the minimization equations are given by

$$\frac{\partial L}{\partial X_b} = \omega z(1 - 2X_b)(1 - f_{ig}) + \alpha\omega vz(1 - 2X_{ig})f_{ig}$$
$$+ v\sigma(\gamma^A - \gamma^B)f_{ig}$$
$$+ RT[\ln(X_b) - \ln(1 - X_b)](1 - f_{ig}) - \lambda(1 - f_{ig}) = 0, \qquad (32a)$$

$$\frac{\partial L}{\partial X_{ig}} = \alpha\omega vz(1 - 2X_b)f_{ig} + v\sigma(\gamma^A - \gamma^B)f_{ig}$$
$$+ \alpha\omega(1 - 2v)z(1 - 2X_{ig})f_{ig}$$
$$+ (1 - 2v)\sigma(\gamma^A - \gamma^B)f_{ig} + \Delta H_{els}f_{ig}$$
$$+ RT[\ln(X_{ig}) - \ln(1 - X_{ig})]f_{ig} - \lambda f_{ig} = 0, \qquad (32b)$$

$$\frac{\partial L}{\partial f_{ig}} = -\omega z X_b(1 - X_b)$$
$$+ \alpha\omega vz(X_b(1 - X_{ig}) + X_{ig}(1 - X_b))$$
$$+ v\sigma\left((X_b + X_{ig})\gamma^A + (1 - X_b + 1 - X_{ig})\gamma^B\right)$$
$$+ \alpha\omega(1 - 2v)zX_{ig}(1 - X_{ig})$$
$$+ (1 - 2v)\sigma(X_{ig}\gamma^A + (1 - X_{ig})\gamma^B) + X_{ig}\Delta H_{els}$$
$$- RT[X_b \ln(X_b) + (1 - X_b)\ln(1 - X_b)]$$
$$+ RT[X_{ig} \ln(X_{ig}) + (1 - X_{ig})\ln(1 - X_{ig})]$$
$$- \lambda(X_{ig} - X_b) = 0, \qquad (32c)$$

$$\frac{\partial L}{\partial \lambda} = X_b(1 - f_{ig}) + X_{ig}f_{ig} - X_0 = 0. \qquad (32d)$$

The solutions for X_b, X_{ig}, and f_{ig} can be readily obtained from Eqs. (32a)–(32d) using standard numerical methods. An example is given in the Appendix using the MAPLE software.[37] The solution for f_{ig} determines the equilibrium grain size from Eq. (12). The solutions for X_b and X_{ig} determine the equilibrium interfacial solute excess from[23,24]

$$\Gamma = \frac{(X_{ig} - X_b)}{\sigma(1 - X_b)}. \qquad (33)$$

III. PARAMETRIC STUDY

Numerical solutions obtained using Eqs. (32a)–(32d) will be presented in this section as a function of the key input parameters ω, ΔH_{els}, X_0, and α. The aim is to show the effect of variation in one parameter while holding the others constant. The fixed (nonvarying) input parameters will be $t = 0.4$ nm, $v = 1/2$, $z = 8$, $\gamma^A = \gamma^B = 0.6$ J/m^2, and $\sigma = 30000$ m^2/mol, The default values for the variable input parameters will be $X_0 = 0.06$, $\omega = -12$ kJ/mol, $\alpha = 5/6$, and $\Delta H_{els} = -110$ kJ/mol. Each of these will be held constant at these values except for the parameter that is currently being varied. The dimension of J/mol is used instead of J/atom which means that Eqs. (32a)–(32d) have been multiplied by Avogadro's number.

A. Interaction energy ω

The ω parameter relates to the atomic bond energies between like and/or unlike pairs of the solute and solvent atoms. The arrows in Figure 2 indicate an increasing (more positive) trend for ω. The segregation tendency increases with more positive ω because AB pairs are less favorable than AA or BB pairs. A nanoscale grain size is therefore stabilized up to higher temperatures in Figure 2(a). As can be anticipated, Figure 2(b) illustrates that at a given temperature the solute excess at the grain boundary is increased with more positive
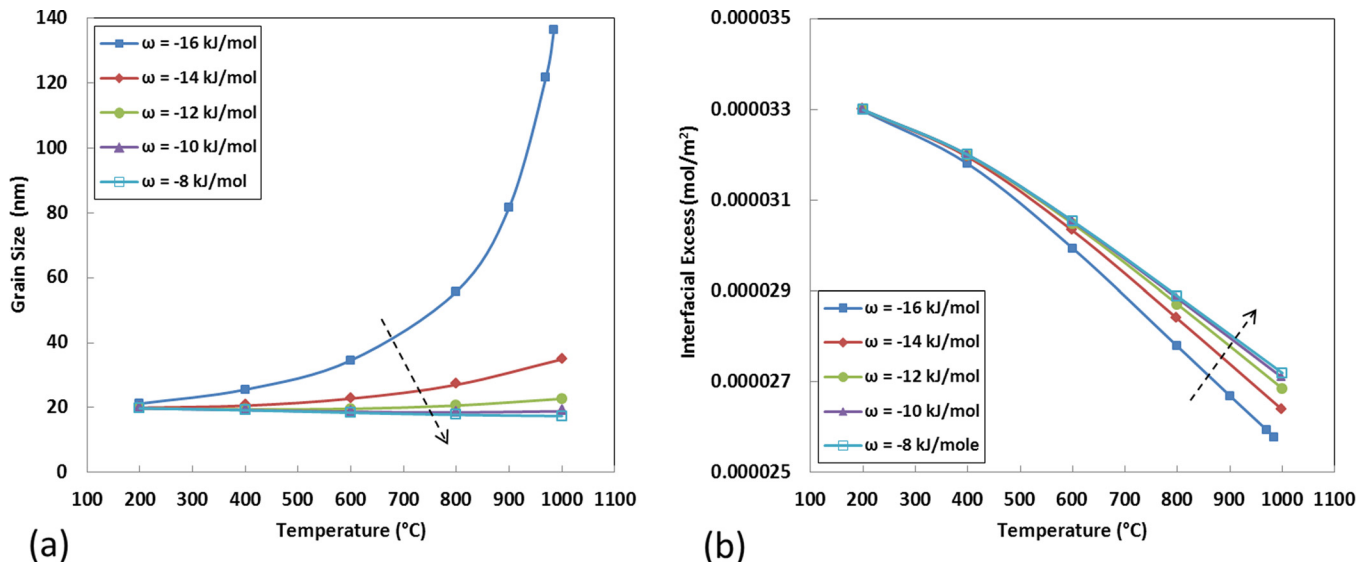

FIG. 2. The effect of interaction energy ω on (a) grain size and (b) interfacial solute excess.
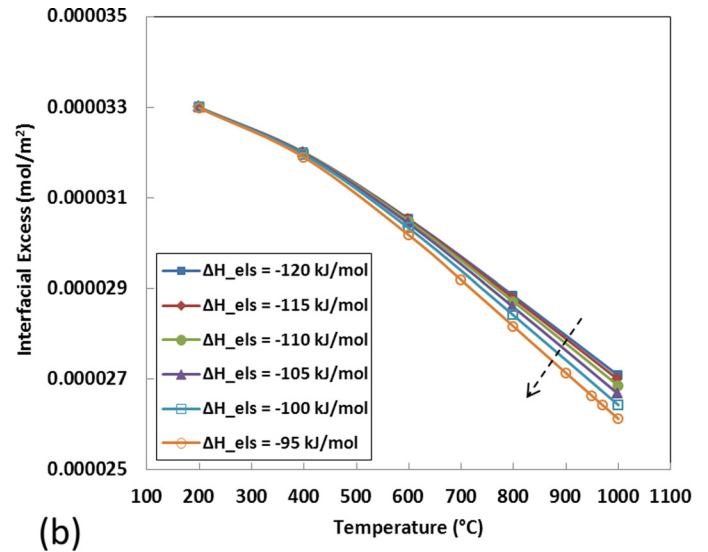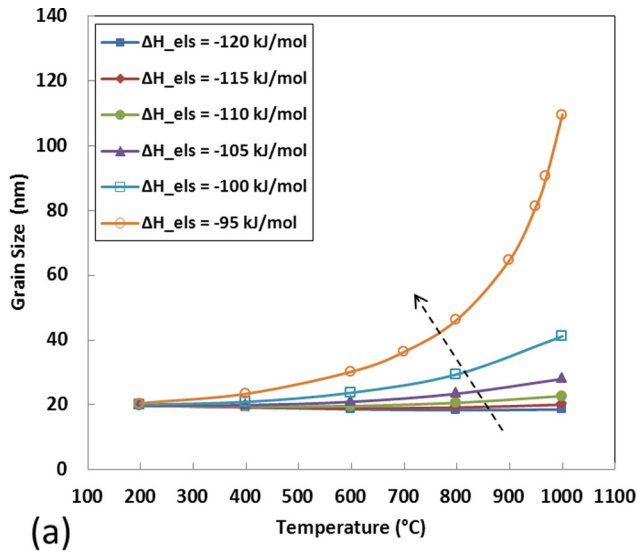
FIG. 3. The effect of elastic enthalpy ΔH_{els} on (a) grain size and (b) interfacial solute excess.

ω. The trend for decreasing solute excess with increasing temperature will always result due to the entropy effect.

B. Elastic strain energy ΔH_{els}

The parameter ΔH_{els} is the (negative) elastic strain energy decrease due to segregation of size misfit solute atoms, and its magnitude is always a driving force for solute segregation. The arrows in Figure 3 indicate a decreasing trend in the magnitude for ΔH_{els}. Figure 3(a) shows that the nanoscale grain size is less stable at higher temperatures when the magnitude decreases. As indicated in Figure 3(b), the interfacial solute excess at a given temperature is also decreased when the magnitude decreases. These effects can be anticipated because the decreasing trend for ΔH_{els} implies a weaker segregation tendency for solute atoms.

C. Global solute content X_0

An increase in the global solute content X_o provides additional solute for segregation to grain boundaries. The arrows in Figure 4 indicate an increasing trend for X_o. With the segregation driving forces (other parameters) held constant, Figure 4(a) shows that a nanoscale grain size is more stable at higher temperatures for increasing X_o. Figure 4(b) shows that the interfacial solute excess at a given temperature is essentially independent of changes in X_o. This behavior is similar to the classical Langmuir-Mclean (or Fowler-Guggenheim) segregation isotherms in which Γ is unaffected by global solute additions.

D. Interaction energy multiplier α

The interaction energy multiplier α plays a role similar to that of the interaction energy parameter ω in Figure 2.
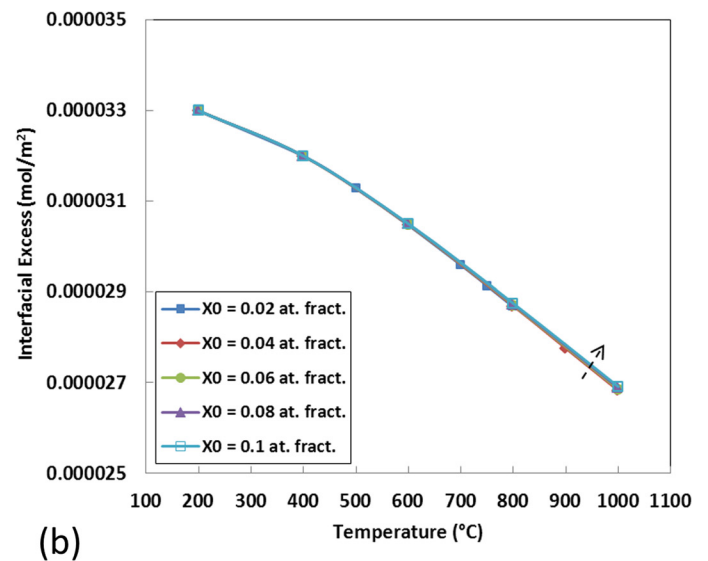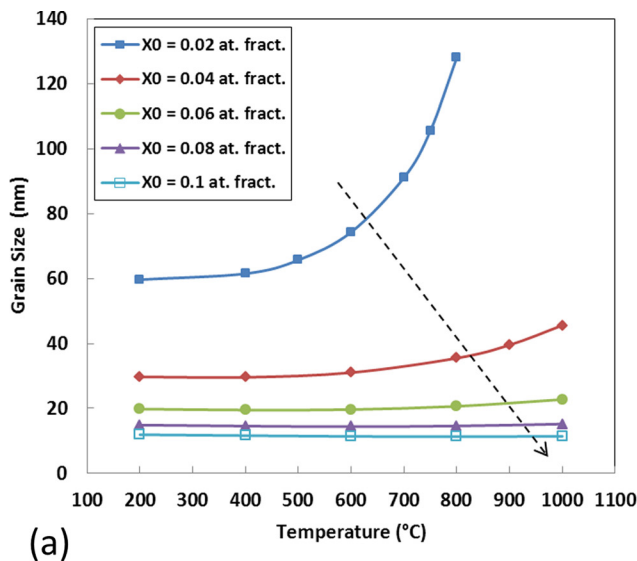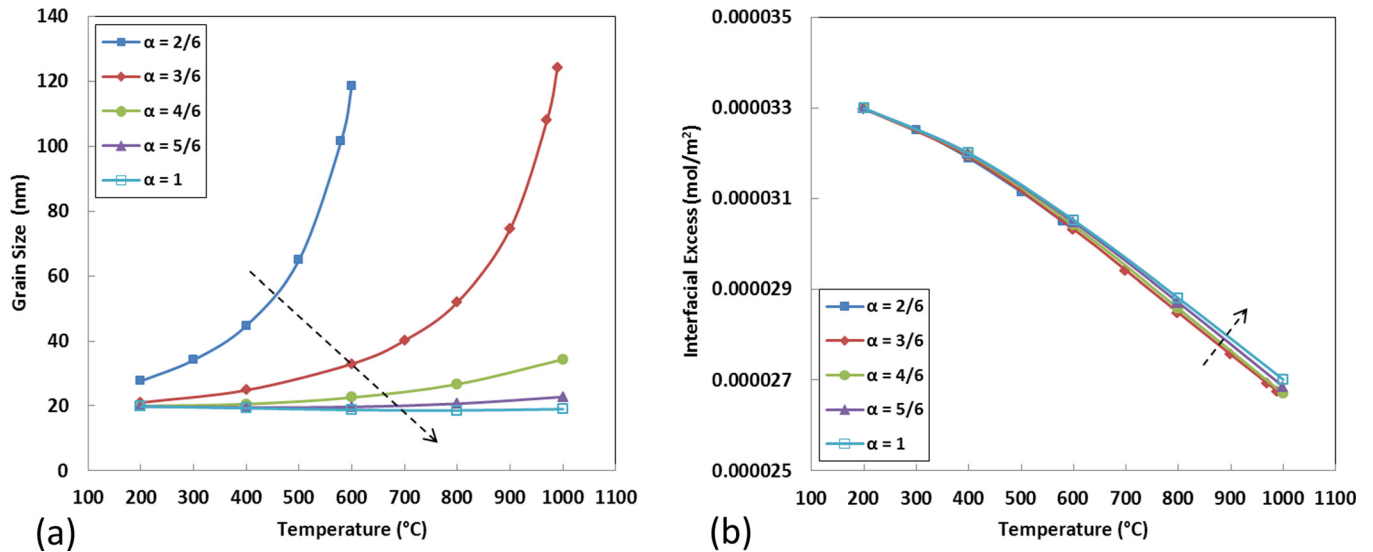

FIG. 4. The effect of global solute content X_o on (a) grain size and (b) interfacial solute excess.

FIG. 5. The effect of the α multiplier on (a) grain size and (b) interfacial solute excess.

The arrows in Figure 5 indicate an increasing (more positive) trend for α. Figure 5(a) shows that when bond energies in the intergranular region approach their counterparts in the bulk region, i.e., α → 1, a nanoscale grain size is more stable at higher temperatures. The effect implies that segregation tendency is enhanced. Figure 5(b) shows that the interfacial solute excess at a given temperature increases somewhat as α → 1, but the effect is not as strong as that in seen Figure 2(b).

IV. RESULTS FOR SELECTED BINARY ALLOYS

In this section, numerical results are presented for several binary alloys that have been investigated in the literature. Thermodynamic stabilization has been suggested as a possible grain-size stabilization mechanism. The values $t = 0.4$ nm, $v = 1/2$, and $\alpha = 5/6$ are used for all the alloys. The grain boundary energy is assumed to be 1/3 of the free surface energy,[25] and the values for γ^A and γ^B are calculated from the free surface energy of pure elements (since surface energy corresponds to a 1/2 broken bond, the grain boundary energy corresponds to a 1/6 broken bond and this sets $\alpha = 5/6$). The elastic strain energy ΔH_{els} and the molar grain boundary area σ are obtained using Eq. (2) (noting that $\Delta H_{els} = -\Delta E_{els}$) and Eq. (20), respectively. In the regular solution approximation for a binary alloy, the interaction energy parameter ω is related to the (chemical) mixing enthalpy ΔH_{mix} by

$$\Delta H_{mix} = z\omega X(1 - X). \tag{34}$$

Therefore, ω can be estimated using the relation

$$\omega = \frac{4}{z}\Delta H^0_{mix}. \tag{35}$$

ΔH^0_{mix} is the enthalpy of mixing for an equimolar ($X = 1/2$) liquid solution of $A + B$. Values of the required parameters for the (solvent-solute) alloy systems Fe-Zr, Cu-Nb, Cu-Zr, and Ni-W were obtained using data available in the literature,[26–28] and these are given in Table I. An extensive

database of ΔH^0_{mix} and ΔE_{els} values for a wide range of solutes in a specified solvent is available in Ref. 29.

The numerical results for the Fe-Zr system are shown in Figure 6. Zr is a very large non-equilibrium solute in Fe, and the experimental Fe-Zr nanocrystalline alloys must be synthesized using non-equilibrium processing methods such as ball milling. The minimum Zr content that retains the grain size in the nanoscale range at 900 °C in Figure 6(a) is 4 at. % Zr. The predicted grain size for Fe-4 at. % Zr annealed at 900 °C is about 100 nm. This compares to the measured TEM grain size for Fe-4 at. % Zr at 900 °C reported by Darling *et al.*,[13] which was about 60 nm. At lower amounts of Zr additions, the thermodynamic grain stabilization is less effective, and the stabilization observed in Ref. 13 in the temperature range up to about 700 °C must be due to contributions from kinetic mechanisms such as solute pining and/or solute drag. Figure 6(b) shows that the solute excess is essentially the same for all Zr contents, similar to the trend seen in Figure 4(b). Based on the solute excess values, the grain boundary atom fraction of solute X_{ig} for the temperature range in Figure 4(b) is about 0.96 for all alloys, and is therefore close to fully saturated grain boundaries. This same trend was observed for the other alloys in Table I, and X_{ig} ranges from about 0.85 to 0.95.

The numerical results for the Cu-Zr system are shown in Figure 7. Zr is again a large non-equilibrium solute, although

TABLE I. Values of the required parameters for the Fe-Zr, Cu-Zr, Cu-Nb, and Ni-W alloys (A = solute).

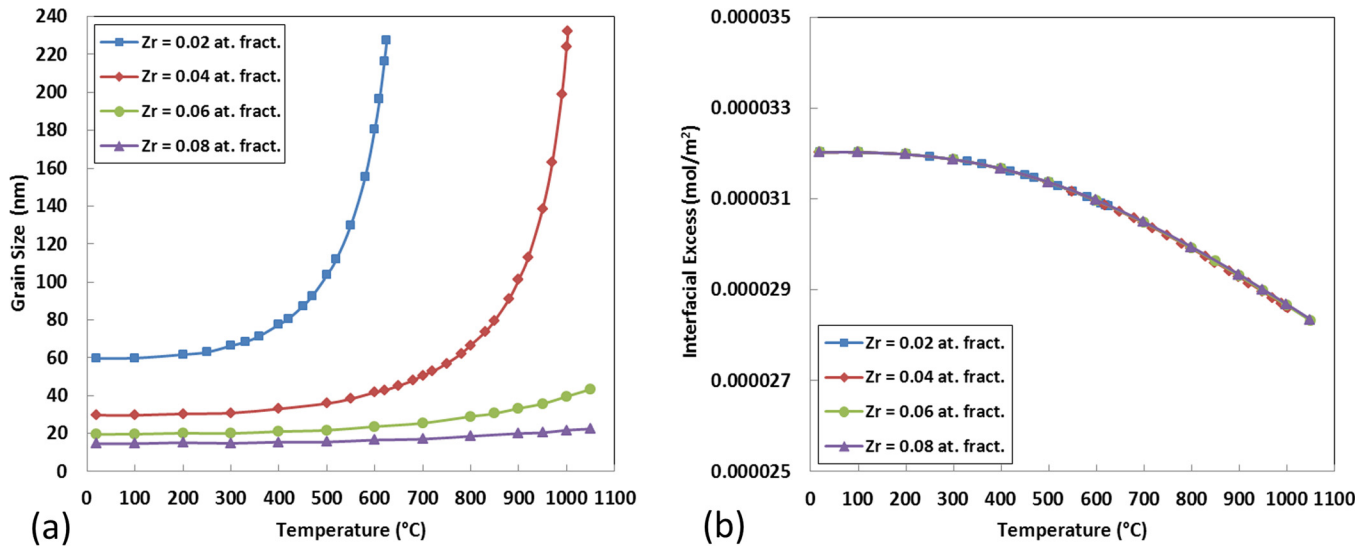| Value	Fe-Zr	Cu-Zr	Cu-Nb	Ni-W
z	8	12	12	12
σ (m²/mol) [Eq. (20)]	31 217	31 222	31 222	29 680
γ^A (J/m²) (Refs. 25 and 26)	0.636	0.636	0.885	1.088
γ^B (J/m²) (Refs. 25 and 26)	0.805	0.602	0.602	0.793
ΔH_{els} (kJ/mol) [Eq. (2)]	−109.3	−90.8	−40.2	−44.3
ΔH^o_{mix} (kJ/mol) (Ref. 27)	−25	−23	+3	−3

FIG. 6. Model predictions of (a) grain size and (b) interfacial solute excess for Fe-Zr alloys.

with a somewhat smaller value of ΔH_{els} and a similar value of ΔH^o_{mix} compared to Fe-Zr. The trends are similar to Figure 6, but more Zr addition is needed to obtain the same level of stabilization. Figure 7(a) indicates that 6 at. % Zr is needed to obtain thermodynamic stabilization in the nanoscale range at 700 °C, compared to somewhat less than 4 at. % Zr in Figure 6(a). Grain size stabilization in the nanoscale range in conjunction with some abnormal grain growth was reported in Ref. 30 for Cu-1 at. % Zr annealed at 900 °C. In this case Figure 7(a) implies an alternate grain size stabilization mechanism, and TEM results showed the presence of nanoscale intermetallic precipitates sufficient to produce additional Zener pinning.[30]

The numerical results for the Cu-Nb system are shown in Figure 8. Nb is a non-equilibrium solute with a significantly smaller value of ΔH_{els} and a slightly positive ΔH^o_{mix}. The former would reduce the effectiveness of thermody-

namic stabilization compared to the Fe-Zr and Cu-Zr systems whereas the latter would enhance the stabilization. Figure 8(a) shows that at the same amount of solute addition, Nb in Cu is less effective than Zr in Cu and both are less effective than Zr in Fe. The experience found with our numerical modeling results is that ΔH_{els} is the dominant factor for thermodynamic stabilization compared to ΔH^o_{mix}. Recent results (to be submitted for publication) obtained in our laboratory demonstrated nanoscale grain size stabilization for 1 at. % Nb in Cu up to 800 °C. Figure 8(a) shows that thermodynamic stabilization is clearly not effective in this case, and HRTEM confirms the presence of Nb nanoscale precipitates in Cu that would be candidates for kinetic stabilization by Zener pinning. Similarly, in the Cu-Ta system, ΔH_{els} and ΔH^0_{mix} values are almost the same as the Cu-Nb system. The numerical calculations show that 10 at. % Ta addition can retain a value of 92 nm nanoscale grain size at 900 °C. This
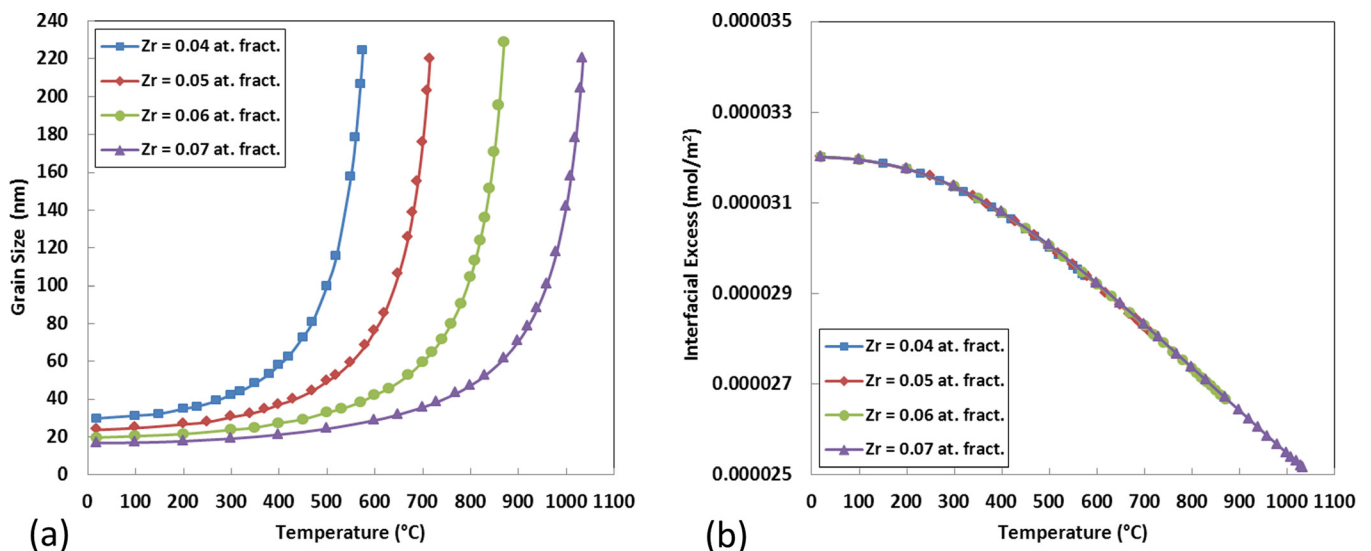

FIG. 7. Model predictions of (a) grain size and (b) interfacial solute excess for Cu-Zr alloys.
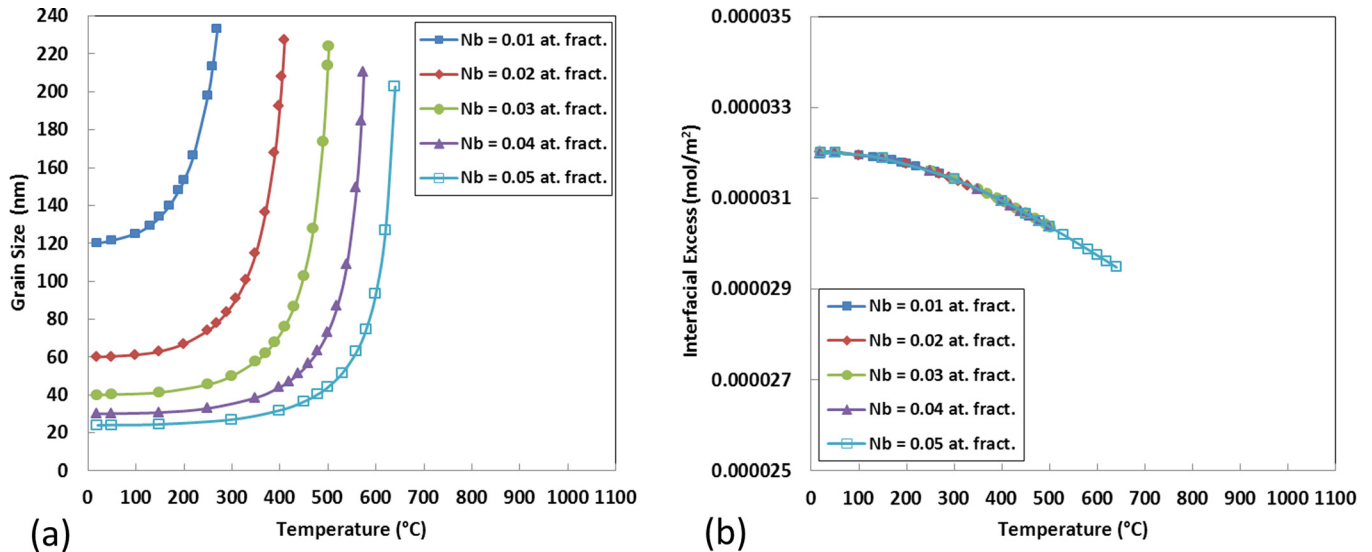
FIG. 8. Model predictions of (a) grain size and (b) interfacial solute excess for Cu-Nb alloys.
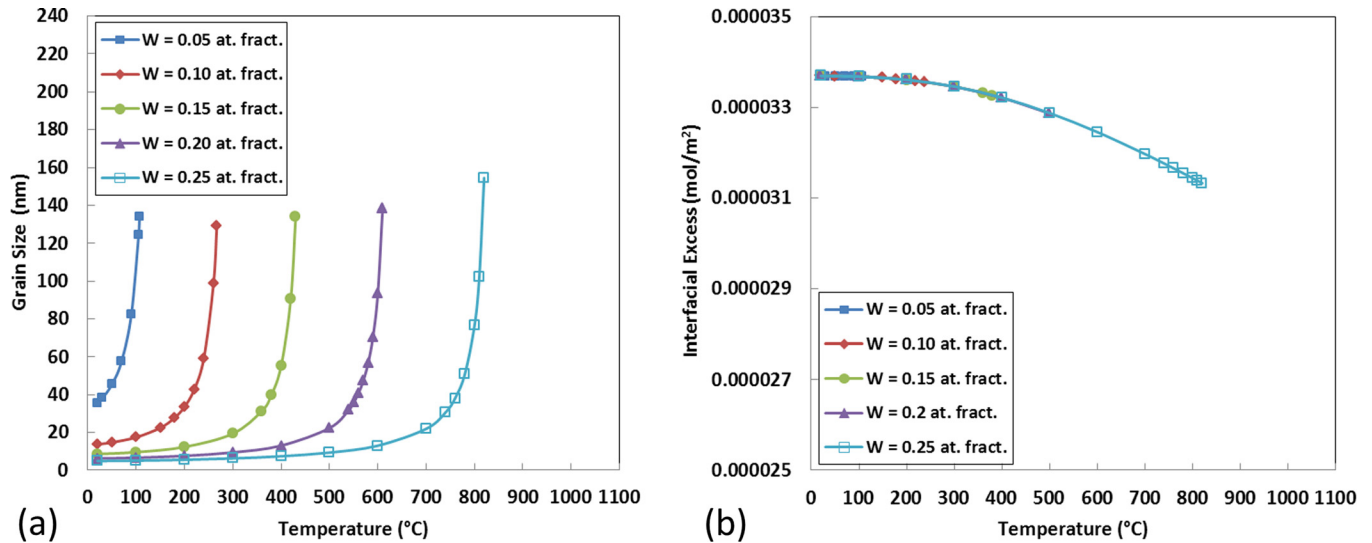

FIG. 9. Model predictions of (a) grain size and (b) interfacial solute excess for Ni-W alloys.

compares well to the experimental result of 111 nm, recently reported by Frolov *et al.*[31] However, the simulated distribution of Ta in Cu-6.5 at. % Ta alloy at high temperatures by molecular dynamic (MD) simulations predicted that Ta diffusion through grain boundaries leads to a distribution of nanoclusters of Ta in the grain boundaries.[31] The Ta nanoclusters contribute to kinetic stabilization mechanisms such as Zener pinning. This is consistent with our model predictions indicating that at 6.5 at. % Ta addition at high temperatures thermodynamic stabilization is not effective.

The numerical results for the Ni-W system are shown in Figure 9. The ΔH_{els} and ΔH^o_{mix} values are similar to those for Cu-Nb, but a comparison of Figures 8(a) and 9(a) shows a significantly different trend. Thermodynamic stabilization in the nanoscale range at 600 °C requires 5 at. % Nb in Cu compared to 20 at. % W in Ni. This is in agreement with experimental results obtained at high temperatures for electrodeposited Ni-W alloys.[32,33] Atom probe tomography

and atomistic simulations in Refs. 34 and 35 indicate a lack of significant W segregation to grain boundaries, implying that thermodynamic stabilization is not effective for Ni-W alloys. However, this work was done using as-plated (un-annealed samples) and is not comparable to results in Figure 9. Atom probe tomography was also reported in Ref. 36, and in this case using annealed Ni-W alloys. W segregation on grain boundaries was observed on nanoscale grain boundaries for Ni-18 at. % W, up to about 700 °C. Above that temperature, extreme grain coarsening was observed. This is in reasonable agreement with Figure 9(a), but is somewhat better grain size stabilization that could be a result of concurrent kinetic mechanisms.

V. SUMMARY AND CONCLUSIONS

Based on the TS approach, a regular solution model was developed to evaluate thermodynamic stabilization of

nanocrystalline grain size in binary alloy systems where non-equilibrium solutes segregate to grain boundaries. An important feature of the present model is that it incorporates elastic strain energy due to size misfit in conjunction with chemical effects. The free energy is properly minimized with respect to simultaneous variation in the grain boundary content and the amount of solute distributed between bulk and grain boundary regions. The Lagrange multiplier method provides minimization equations that can be solved using standard numerical methods, and an example solution is provided. Using data available in the literature, numerical results were obtained for several binary alloys systems that have been investigated experimentally, and where thermodynamic stabilization might be expected. While both strain energy and chemical effects are possible, it appears that the former dominates in strongly segregating systems. Although it is not expected that a regular solution model can make exact predictions of the temperature and solute ranges over which thermodynamic stabilization of nanoscale grain size can occur, the trends are significant. There are competing kinetic stabilization mechanisms when non-equilibrium solutes are present. These include solute pinning or drag, and Zener pinning by precipitates. The formation of the latter competes with solute segregation to the grain boundaries and the effects are dependent on processing time-temperature paths and diffusion rates. In the numerical results presented here for several alloy systems, there are cases where the model predictions are in good agreement with experimental results and thermodynamic stabilization is viable. In other cases, the model predictions are not even close, but nonetheless are useful indications that kinetic stabilization effects must be present. A more complete understanding and exploitation of the stabilization of nanoscale grain size at high temperatures by solute additions must take into account both thermodynamic and kinetic stabilization mechanisms, along with time-temperature paths used for processing. Direct confirmation of grain boundary segregation, using techniques like atom probe tomography or high-resolution electron microscopy, has been done only in a few investigations, but it will be essential for further identification of the stabilization mechanisms and verification of the stabilization models.

ACKNOWLEDGMENTS

[1] C. Koch, R. Scattergood, K. Darling, and J. Semones, J. Mater. Sci. **43**, 7264 (2008).
[2] J. Weissmüller, Nanostruct. Mater. **3**, 261 (1993).
[3] J. Weissmuller, J. Mater. Res. **9**, 4 (1994).
[4] E. D. Hondros, *in Energetics of Solid-Liquid Interfaces* (Butterworth, London, 1969), p. 77.
[5] B. Färber, E. Cadel, A. Menand, G. Schmitz, and R. Kirchheim, Acta Mater. **48**, 789 (2000).
[6] J. Weissmüller, W. Krauss, T. Haubold, R. Birringer, and H. Gleiter, Nanostruct. Mater. **1**, 439 (1992).
[7] C. D. Terwilliger and Y.-M. Chiang, Acta Metall. Mater. **43**, 319 (1995).
[8] Y. R. Abe and W. L. Johnson, Mater. Sci. Forum **88–90**, 513 (1992).
[9] E. Ma, Minerals Metals and Materials Society, Chemistry and Physics of Materials Committee, Minerals Metals and Materials Society, Thermodynamics and Phase Equilibria Committee, and Minerals Metals and Materials Society Meeting, *Chemistry and Physics of Nanostructures and Related Non-Equilibrium Materials* (The Society, Warrendale, PA, 1997).
[10] C. E. Krill, R. Klein, S. Janes, and R. Birringer, "Mechanically alloyed and nanocrystalline materials," Mater. Sci. Forum **179**, 443 (1995).
[11] C. E. Krill, H. Ehrhardt, and R. Birringer, Z. Metallkd. **96**, 1134 (2005).
[12] B. K. VanLeeuwen, K. A. Darling, C. C. Koch, R. O. Scattergood, and B. G. Butler, Acta Mater. **58**, 4292 (2010).
[13] K. A. Darling, B. K. VanLeeuwen, C. C. Koch, and R. O. Scattergood, Mater. Sci. Eng., A **527**, 3572 (2010).
[14] D. McLean, *Grain Boundaries in Metals* (Clarendon, Oxford, 1957).
[15] J. Friedel, Adv. Phys. **3**, 446 (1954).
[16] R. Defay, I. Prigogine, and A. Bellemans, *Surface Tension and Adsorption* (Longmans, London, 1966).
[17] J. J. Burton and E. S. Machlin, Phys. Rev. Lett. **37**, 1433 (1976).
[18] P. Wynblatt and R. C. Ku, Surf. Sci. **65**, 511 (1977).
[19] P. Wynblatt and D. Chatain, Metall. Mater. Trans. A **37**, 2595 (2006).
[20] J. R. Trelewicz and C. A. Schuh, Phys. Rev. B **79**, 094112 (2009).
[21] T. Chookajorn, H. A. Murdoch, and C. A. Schuh, Science **337**, 951 (2012).
[22] G. Palumbo, S. J. Thorpe, and K. T. Aust, Scr. Metall. Mater. **24**, 1347 (1990).
[23] A. P. Sutton and R. W. Balluffi, *Interfaces in Crystalline Materials* (Clarendon, Oxford, 1995).
[24] O. C. Hellman and D. N. Seidman, Mater. Sci. Eng., A **327**, 24 (2002).
[25] D. A. Porter, K. E. Easterling, and M. Sherif, *Phase Transformations in Metals and Alloys*, 3rd ed. (CRC/Taylor & Francis [distributor], Boca Raton, FL/London, 2009).
[26] W. R. Tyson and W. A. Miller, Surf. Sci. **62**, 267 (1977).
[27] L. Vitos, A. V. Ruban, H. L. Skriver, and J. Kollár, Surf. Sci. **411**, 186 (1998).
[28] F. R. d. Boer, *Cohesion in metals : transition metal alloys* (Elsevier Scientific, New York, U.S.A., 1988).
[29] M. Atwater and K. Darling, ARL-TR-6007, May 2012 ed., ARL, 2012.
[30] M. Atwater, "Stabilizing Nanocrystalline Copper and Brass by Solute Addition," Ph.D. dissertation (North Carolina State University, 2012).
[31] T. Frolov, K. A. Darling, L. J. Kecskes, and Y. Mishin, Acta Mater. **60**, 2158 (2012).
[32] T. Yamasaki, P. Schloβmacher, K. Ehrlich, and Y. Ogino, Nanostruct. Mater. **10**, 375 (1998).
[33] T. Yamasaki, Scr. Mater. **44**, 1497 (2001).
[34] A. J. Detor, M. K. Miller, and C. A. Schuh, Philos. Mag. **86**, 4459 (2006).
[35] A. J. Detor and C. A. Schuh, Acta Mater. **55**, 4221 (2007).
[36] P. Choi, T. Al-Kassab, F. Gärtner, H. Kreye, and R. Kirchheim, Mater. Sci. Eng., A **353**, 74 (2003).
[37] See supplementary material at http://dx.doi.org/10.1063/1.4791704 for a numerical solution of equilibrium grain size and interfacial solute excess using the Maple software.